PHYSICAL REVIEW A VOLUME 24, NUMBER 2 AUGUST 1981

K-shell ionization probability in close collisions of 7–12-MeV protons with targets of $Z = 24$ –83

M. Dost, S. Hoppenau, J. Kising, S. Röhl, and P. Schorn
Institut für Kernphysik, University of Köln, D-5000 Köln 41, Germany
(Received 27 January 1981)

K-shell ionization probabilities were measured by the particle–x-ray coincidence technique for 7-MeV protons of 15 to 39 fm impact parameter on 24 targets from Cr to Bi. For 22 of these targets, total K-shell ionization cross sections are also reported. Additional K-shell ionization probabilities were measured for 7-, 10-, and 12-MeV protons on Mo, Cd, and Sn, at impact parameters down to 2 fm. While the total K-shell cross sections closely follow relativistic semiclassical (RSCA) calculations supplemented by minor binding-plus-polarization corrections, significant discrepancies of up to 70% occur for the K-shell ionization probabilities at small impact parameters, particularly for the targets from Cr to Zr. They can be traced back to the use of hydrogenic wave functions in the RSCA calculation, whereas nuclear recoil may account only for a few percent of the discrepancies. The data on both K-shell total cross sections and ionization probabilities exhibit the pattern characteristic for small distortions of the K-electron binding energy by the projectile charge: adiabatic binding for $\xi_K < 1$ and nonadiabatic polarization for $\xi_K > 1$. The perturbed-stationary-state approximation somewhat underestimates these distortion effects.

I. INTRODUCTION

The wealth of inner-shell ionization cross-section data[1] has, in recent years, been complemented by various sets of data on impact-parameter-dependent ionization probability. As far as the K-shell ionization by low-charge projectiles is concerned, the situation may be characterized as follows: The semiclassical treatment based on first-order time-dependent perturbation theory[2] (SCA) accounts on the whole quite satisfactorily for the existing data on collisions with impact parameters large compared to the dimensions of the atomic nucleus, and consequently on total cross sections. In such situations, it has been demonstrated that SCA is able to yield predictions of K-shell ionization probabilities[3–9] usually within experimental errors if proper account is taken of the relativistic motion of the K-shell electrons, of the effects of the projectile trajectory through the electron distribution of the atom, and of increased or reduced electron binding owing to the temporary presence of the projectile charge in the atom. In most of these cases it has been found sufficient to represent the active electron by hydrogenic wave functions adapted to the real atom by use of an effective charge Z_{eff}. Closer collisions, especially at high relative velocity v_p/v_K (where v_p is the projectile velocity and v_K the K-electron velocity), require that proper attention be paid to the screening effects[10,11] in both the bound and the free-electron wave functions. Striking improvement has been obtained through the use of Hartree-Fock (HF) wave functions in semiclassical calculations of protons on Ag (Ref. 12) down to impact parameters $b = 95$ fm, i.e., $b/r_K = 0.08$, with r_K the Bohr radius of the K shell. Similarly, the use of HF wave functions has also improved agreement with the data for other collision systems.[11, 13–15]

There has recently arisen the need to know K-shell ionization probabilities in still closer collisions: at impact parameters b comparable to the nuclear radius, with typically $b/r_K = 0.01$–0.02. In the analysis of experiments[16] aimed at measuring the compound nuclear width relative to the K-vacancy width, knowledge of the K-shell ionization probability P_K in such central collisions is required at energies above the nuclear Coulomb barrier. Very few experimental data on such collisions are known[7,14,15,17–19]; and the impression prevails that in those examples agreement of theory with experiment is much less satisfactory than has become customary in more distant collisions.

Apart from the need to analyze the above-mentioned compound-nucleus measurements, we feel that a study of K-shell ionization in central collisions is a worthwhile subject of study for its own sake. We have chosen for projectiles protons of 7 to 12 MeV, and targets between Cr ($Z = 24$) and Bi ($Z = 83$) in order to obtain a data set that would span a wide enough range for systematic trends to be discernible. Experimental conditions were arranged such that the impact parameter was only a few fm for each collision system throughout the data series. These experimental conditions do not allow us to measure at the same time the variations P_K with the impact parameter. The chosen cut through the $P_K(b, Z)$ surface thus concentrates on close collisions. However, integrated K-shell cross sections σ_K were taken at the same time. A preliminary account of parts of this work was previously given in Refs. 20 and 21.

After describing the experimental technique

in Sec. II we will mention some problems of data analysis in Sec. III, and present the results of the measurements in Sec. IV. A discussion of the data and of the remaining discrepancies with calculations is given in Sec. V. There the probable origin of the remaining difficulties in describing nonadiabatic, very asymmetric, central collisions with K-shell ionization is singled out. Conclusions are summarized in Sec. VI.

II. EXPERIMENTAL TECHNIQUE

The data series from $Z = 24$ to 83 to be presented in Sec. IV could not be obtained in one single geometry and detector setup. Energies of K x rays vary from about 5 to 90 keV so that the use of different detectors is necessary. The x-ray production cross section decreases by approximately a factor 10^4. Consequently, count rate conditions and real-to-random coincidence ratios change drastically. Finally, the particle scattering angle had to be adapted to the particular Z in question in order to maintain the impact parameter close to a fixed value.

A schematic view of the mechanical setup is shown in Fig. 1. The collimated proton beam from the HVEC FN-tandem of the University of Köln strikes the tilted target before passing on to a secondary target of Au or Ta and to the beam stop 0.5 and 5.5 m downstream. Shown in Fig. 1 is the high-Z situation where the coincident x-ray spectra are taken by an 1140-mm^2 area and 4-mm thick NaI(Tl) scintillator behind a 1-mm lucite window and coupled to a Hamamatsu 2060 phototube. A 200-mm^2 area and 5-mm thick Si (Li) x-ray detector with its 1-mm lucite absorber is brought into the vacuum chamber through an O-ring seal. It serves as an efficiency standard for the NaI(Tl) detector and also checks target purity.

Scattered particles are detected in three 1000-μm silicon surface barrier detectors behind a half-circular aperture at angle θ_p, covered by 7-μm aluminum. There is a $\theta = 90°$ particle monitor placed below the Si(Li) detector. Measurements for $Z \leq 40$ are done with the front window of the Si(Li) detector only 2 mm from the target spot, and the NaI(Tl) removed. For the back-angle measurements on Mo, Cd, and Sn a 1.64-sr particle detector at $\theta_p = 130 \pm 30°$ is added which consists of two 450-mm^2 area and 1000-μm surface barrier detectors above and below the center plane (for details, see Ref. 16).

The protons are produced in an rf ion source, and their intensity is limited to typically 50 pA on target to prevent overloading of the particle (high Z) or x-ray (low Z) detectors. The beam is continuously monitored for possible high-frequency intensity modulations, by the two particle detectors viewing the secondary target (Fig. 2). The time spectrum of left-right coincidences of elastic protons maps the time structure of the proton beam. Examples are shown in Fig. 3 both for the rf and a duoplasmatron ion source. It is seen that the duoplasmatron beam is not sufficiently constant to allow reliable subtraction of random coincidences. A list of targets and their characteristics is given in Table I. The proton-x-ray coincidences from double scattering events in low-Z systems[21] are minimized by choosing thin targets, when possible self-supporting. The correction of the elastic proton peak for scattering from carbon and oxygen is determined from the 90° monitor spectrum and the forward-over-90° ratio, measured separately on carbon and mylar targets.

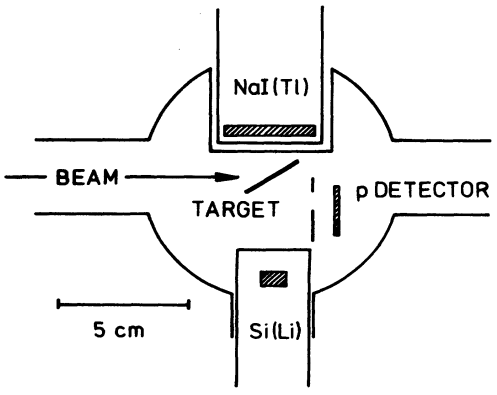

FIG. 1. Mechanical setup of detectors and target. Depicted is the situation wherein high-Z target x rays are measured by the NaI(Tl) scintillator while the Si(Li) detector in the distant position serves for both normalization and target purity check. The particle (p) detector is an array of three surface-barrier detectors behind an aperture having the form of a half-circular slot.

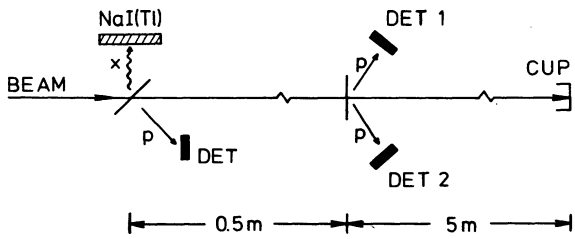

FIG. 2. Schematic layout of detector arrangements at both the primary and secondary targets. The time spectrum of coincidences between elastic particles in detectors DET1 and DET2 serves to monitor the time structure of the accelerator beam.

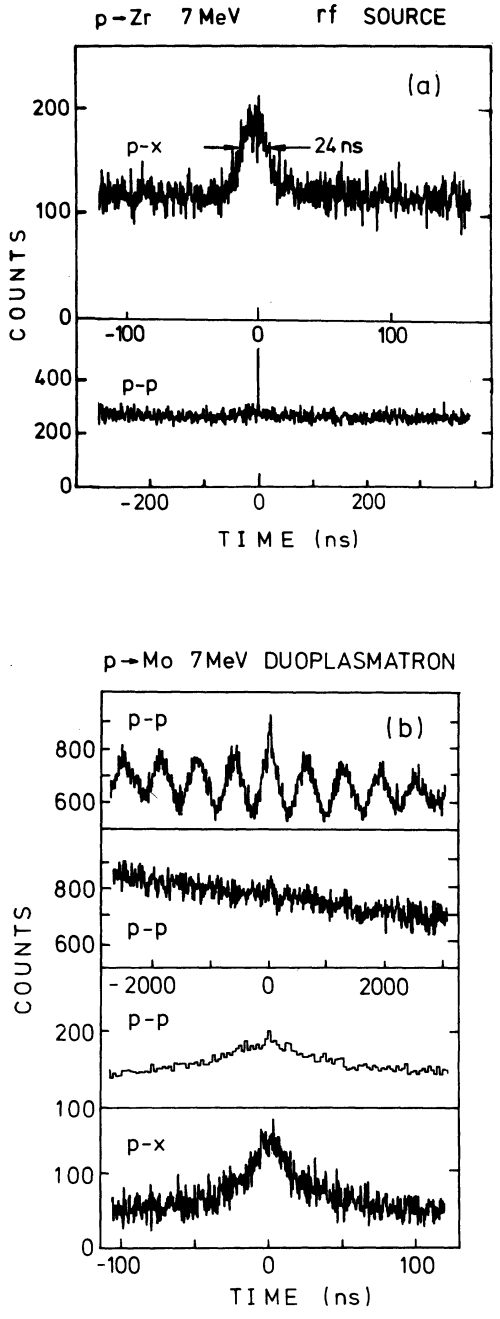

FIG. 3. Examples of time spectra of p-x and elastic p-p coincidences. Part (a) shows conditions with the beam from an rf proton source. The spike in the p-p part of the figure results from prompt events with very low energy signals, probably electrons. Part (b) shows conditions often met with a duoplasmatron ion source. The upper two time spectra show the influence of different source conditions. The lower two show the residual time structure in both p-p and p-x under "good" source conditions. Reliable integration of the real p-x coincidences is not possible in this situation.

TABLE I. Target information. No attempt at an accurate determination of areal density is made where the double-scattering correction (see text) is seen to be smaller than 2%. (Se is the only exception, as the target was destroyed before a more accurate thickness measurement was made.)

Target[a]	Areal density ($\mu g/cm^2$)
$_{24}Cr$	61,67,135[b]
$_{26}Fe(C)$	8[b]
$_{28}Ni$	28[b]
$_{29}Cu$	97[b]
$_{30}Zn$	182[b]
$_{34}Se$	150[d]
$_{38}Sr(C)$	17[c]
$_{40}Zr$	511,600[b]
$^{92}_{42}Mo$	331,552[b]
$_{44}Ru$	15[d]
$_{47}Ag$	50[d]
$^{106}_{48}Cd$	900[b]
$^{112}_{50}Sn$	100,200,314[b]
$^{130}_{52}Te(C)$	65[c]
$_{56}Ba(C)$	77[c]
$_{58}Ce(C)$	92[c]
$_{62}Sm$	50[d]
$^{165}_{67}Ho$	60[d]
$^{169}_{69}Tm$	65[d]
$_{73}Ta$	150[d]
$_{78}Pt$	50[d]
$^{197}_{79}Au$	60[d]
$_{82}Pb$	100[d]
$^{209}_{83}Bi$	90[d]

[a] Natural isotopic composition and self-supporting foil, except when specified otherwise; (C) indicates carbon backing.
[b] ± 10% or less.
[c] ± 15%.
[d] ± 50%.

The measurement of x-ray-detector efficiency in the very close geometry presents a difficulty. It is not possible with sufficient accuracy to reproduce size and position of the beam spot on the target by calibrated x-ray sources. At a distance of 30 mm between front window and source, however, the efficiency of the 200-mm² Si(Li) detector is measured to better than 5% using the

calibrated sources listed in Table II. (These calibrated sources are purchased from Bureau National de Métrologie des Rayonnements Ionisants, Saclay, France, and from Physikalisch-Technische Bundesanstalt, Braunschweig, Germany.) Uncertainties due to source position are here below 2%. The x-ray intensities in close geometry are then normalized to the Si(Li) detector in the 30-mm position from the beam spot on target, with Si(Li) dead time kept to zero.

The electronic signal processing is largely conventional, using fast-slow coincidence technique with constant-fraction timing and event-mode recording by a PDP-11-20 computer. The time resolution (full width at half maximum) varies from 82 to 24 ns from Cr (5.4 keV) to Zr K x rays (15.7 keV) with the Si(Li) detector, and from 5.1 to 3.3 ns from Zr to Bi K x rays (77 keV) with the NaI(Tl) detector. Better time resolution (40 ns for Fe, 6.4 keV; and 12.3 ns for Sn, 25.3 keV) can be obtained with the Si(Li) detector. With the singles count rates limited to 10 kHz in both x-ray and particle detectors, the real-to-random coincidence ratio varies from 0.15 (Cr) to 1.0 (Cd) to 8.3 (Au). The most serious problems with random coincidence background arise for proton backscattering at $\theta_p = 130°$ and high collision energy (12 MeV), owing to the extreme disparity between very small proton rate and high x-ray rate. Special attention to a proton beam without any time structure is then required, and very long running times cannot be avoided.

TABLE II. Sources and photon energies used in the efficiency calibration of the x-ray detectors.

Source	Photon energies used in efficiency calibration (keV)
^{49}V	4.5; 4.9
^{55}Fe	5.9; 6.5
^{57}Co	6.4; 7.1; 14.4; 122.0; 136.0
^{65}Zn	8.04; 8.94
^{85}Sr	13.4; 15.0
^{241}Am	13.9; 17.8; 20.8; 26.4; 59.54
^{93}Nb^{m}	16.6; 18.6
^{109}Cd	22.1; 24.9; 87.7
^{113}Sn	24.2; 27.3
^{133}Ba	30.9; 35.0; 81.0
^{182}Ta	31.7; 58.9; 67.8; 84.7
^{137}Cs	32.1; 36.5
^{152}Eu	39.9; 45.4
^{159}Dy	43.74; 44.47; 50.39; 51.74

III. DATA ANALYSIS

We shall mention here only those few points that do not necessarily form part of the standard data treatment. We choose to normalize the data in such a way that dead-time measurements are unnecessary. The ionization probability is given by

$$P_K = \frac{N_c}{N_p} F$$

with F being the normalization, N_c the number of coincidences of scattered protons with K x rays, and N_p the number of detected scattered protons. For isotropic emission of the K x radiation, the normalization F can be expressed as

$$F = \frac{N_x^r}{N_x \omega_K (\Omega_x^r/4\pi)}$$

with N_x^r the number of K x rays detected in the distant reference x-ray detector of efficiency Ω_x^r, possibly normalized via a particle monitor to the main run, ω_K the K-shell fluorescence yield,[22] and N_x the number of K x rays registered by the detector at close distance. The dead-time correction factors of N_c and $N_p N_x$ cancel so that P_K is obtained without dead-time measurement if both N_x^r and the pulse-height–analyzer system are free of dead time. These conditions are sufficiently well fulfilled as coincidence rates are a few Hz, and downgraded singles rates below 1 kHz. The x-ray count rate in the reference detector is always kept below 0.1 kHz.

A second point concerns ionizing double-scattering events in targets of finite thickness. The correction formula given in Ref. 21 is generalized[23] to take into account the azimuthal dependence of target-layer thickness seen by the scattered protons. The net correction is calculated[23] by integrating over the geometrical boundaries of the actual particle detectors. A list of net correction factors P_K/P_K^{uncorr} is given in Table III. We note that, other things being equal, the double-scattering correction becomes more pronounced with increasing projectile energy.

For the targets of ^{nat}Sm, ^{165}Ho, ^{169}Tm, and ^{181}Ta, the intensity due to internal K-shell conversion after inelastic nuclear excitation has to be subtracted from the coincident spectra. Unfolding of the coincident particle spectra is possible in all these cases as the energy separation of protons after inelastic nuclear scattering and after elastic scattering with K-shell ionization is at least 39 keV. The case of ^{197}Au is different in that energy loss by K-shell ionization (80.71 keV) differs only little from energy loss by excitation of the 77-keV ($\frac{1}{2}^+$) nuclear state, and that also the de-excitation gamma ray cannot be dis-

TABLE III. Corrections for double scattering in the measurement of P_K. Given are the fractions $D=1-(P_K/P_K^{\text{uncorr}})$, P_K^{uncorr} being the uncorrected ionization probability. Not listed are the cases where $D \leq 0.02$.

Target	E_p (MeV)	θ_p (deg)	D
Cr	7	13	0.12–0.25[a]
Ni	7	21	0.04
Cu	7	21	0.18
Zn	7	21	0.23
Se	7	21	0.14
Zr	7	21	0.30
Mo	7	15	0.21
	7	130	0.21
Cd	7	30	0.28
	7	130	0.25
Sn	7	15	0.05
	7.138	130	0.05
	10	15	0.06
	10	130	0.03
	12	15	0.06
	12	130	0.05

[a] For different target thicknesses.

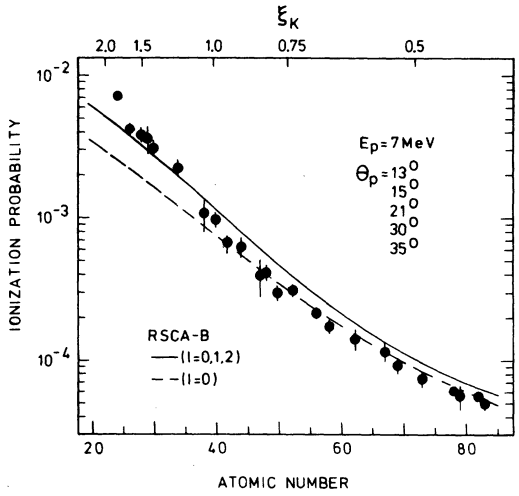

FIG. 4. K-shell ionization probabilities of targets from $_{24}$Cr to $_{83}$Bi by 7-MeV protons. The scale of reduced velocity ξ_K, defined in Sec. IV, is indicated. Impact parameter is near 20 fm throughout the whole range of targets; the scattering angle θ_p was chosen accordingly for the different atomic numbers. The curves represent relativistic semiclassical calculations corrected for binding (RSCA-B). The dashed curve includes only monopole ($l=0$) transitions into the continuum, the solid curve takes also dipole ($l=1$) and quadrupole ($l=2$) transitions into account.

tinguished from the Au K x rays by the NaI(Tl) detector. However, by using the differential Coulomb excitation cross section[24, 25] and internal conversion coefficients, a contribution of only 1% to the proton-x-ray coincidence rate by the 77-keV gamma rays is calculated.

The integrated K-shell ionization cross sections σ_K are derived from the measurements using the known electronic demultiplication of the x-ray singles rates, and the particle spectra at 21° for $Z=24$–40 and at 90° for $Z=40$–83, normalized to optical-model[26] elastic cross sections.

IV. RESULTS

The measured K-shell ionization probabilities at 7 MeV are summarized in Fig. 4. They range from 5×10^{-5} for Bi to 7.3×10^{-3} for Cr. The particle scattering angle has been varied according to target atomic number Z so as to maintain the classical impact parameter $b=(Ze^2/2E_p)\times\cot\frac{1}{2}\theta_p$ in the vicinity of 20 fm, with E_p and θ_p the proton energy and particle scattering angle, respectively. The angle 15° applies to the targets Cr and Fe and to Mo and Sn; the 21° refer to Ni, Cu, Zn, Se, Sr, Zr; the 30° correspond to Ru, Ag, Cd, Te, Ba, Ce; and the angle 35° applies to all heavier targets, i.e., Sm, Ho, Tm, Ta, Pt, Au, Pb, and Bi. Thus, the impact parameter defined by these scattering angles varies between $b=(15\pm7)$ fm for Ni to (39 ± 19) fm for Sn, but is in most cases much closer to 20 fm throughout the data set of Fig. 4. The uncertainty attached to the value of b is combined in quadrature from the classical uncertainty

$$\Delta b_1=\frac{Ze^2}{4E_p}\sin^{-2}\left(\frac{\theta_p}{2}\right)\Delta\theta_p$$

due to the finite angular aperture $\Delta\theta_p$, and the quantum-mechanical uncertainty[27]

$$\Delta b_2=\left[\lambda\!\!\!^{-}_p\frac{Ze^2}{4E_p}\sin^{-2}\left(\frac{\theta_p}{2}\right)\right]^{1/2},$$

with $\lambda\!\!\!^{-}_p$ the projectile rationalized de Broglie wavelength. Net uncertainties are between $\Delta b=\pm7$ fm for Ni and $\Delta b=\pm19$ fm for Sn, and quite generally of the order of b itself. The atomic-number scale in Fig. 4 is supplemented by a reduced-velocity (ξ_K) scale,[28, 29] where $\xi_K=(2/\theta_K)\times v_p/v_K$, θ_K being the screening constant,[10] and v_K the Bohr velocity of the target K electron. The experimental errors amount on the average to about 15%, with exceptions for Ag (30%), Au (20%), Cr (10%), Ba (8%), and Pt (9%). In most cases, the main sources of error are uncertainties in x-ray-detector efficiency and the subtraction of random coincidences. For Sm, Ho, Tm, and Ta, unfolding in the coincident particle spec-

tra (see Sec. III) contributes an additional uncertainty. The theoretical curves in Fig. 4 will be explained in Sec. V.

Ionization probabilities in forward and backward scattering for 7-, 10-, and 12-MeV protons are compared in Fig. 5. The selection of cases is motivated by the interest to study ionization in compound nuclear scattering.[16] The data points for Cd and Sn at 130°, measured at 7.138 MeV to avoid nearby isobaric analog resonances, are plotted together with the 7-MeV 15 and 30° points which appear already at $Z = 48$ and 50 in Fig. 4. The dominating source of error in the 130° data points, besides statistics of the number of real coincidences (20%), is the uncertainty in the subtraction of random coincidences, the real-to-random ratio being only about 0.1 at back angles. Residual time structure, if present, then enters sensitively and must be corrected for. The amount of random coincidences accumulated at the position of the prompt peak depends on ion source conditions. The measured fractions of such accumulated randoms, even for the rf ion source, amount to 0.22 for Mo, 0.26 for Cd, and 0.51 and 0.42 for Sn at 7 and 10 MeV, respectively, and are negligible otherwise. In particular, at identical beam conditions, the forward-angle data points remain unaffected owing to the higher real-to-random coincidence ratios. The corrections, though sizable in the cases listed above, are measured with good statistical accuracy, except for Sn at 10 MeV and for Mo where they give the largest contribution to the net error. Again, theoretical curves in Fig. 5 will be discussed in Sec. V.

Finally, Fig. 6 shows the K-shell ionization cross sections at 7 MeV for 22 of the 24 elements of Fig. 4, plotted over atomic number and, alternatively, relative velocity ξ_K. No cross sections are given for Fe and Sr. The error bars vary from an average of 12% below Zr, to 16% between Zr and Ce, to 12% again between Ce and Bi. They receive their largest contribution from the uncertainty of the optical-model elastic cross sections serving for normalization. The K-shell cross sections compare, on the whole, quite well with values available in the literature: They agree within error bars with the values given by Bissinger *et al.*[30] for Ag, and by Akselsson and Johannsson[31] for Ni, Cu, and Ag. The cross section for Ta is 39% above that given by Berinde *et al.*,[32] and the value for Pb is 32% above the result of Laegsgaard *et al.*[9] For both Ta and Pb the two-standard-deviation errors would overlap. The theoretical curve in Fig. 6 will be explained in Sec. V. The data of Figs. 4–6 are summarized in numerical form in the Appendix.

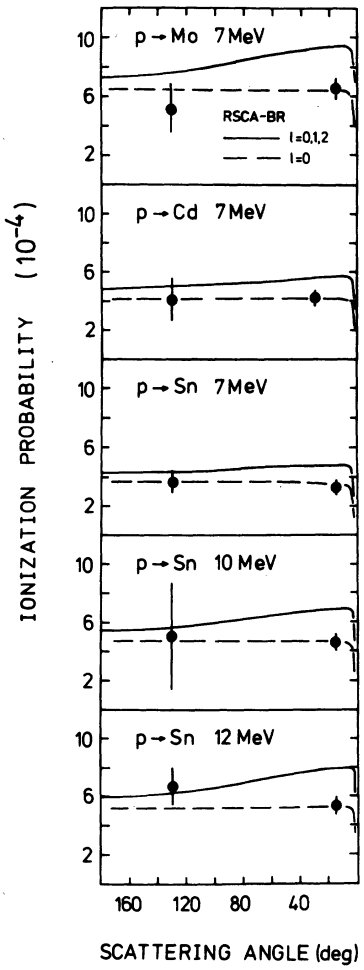

FIG. 5. K-shell ionization probabilities in forward and backward scattering of 7-, 10-, and 12-MeV protons on $_{50}$Sn, and of 7-MeV protons on $_{42}$Mo and $_{48}$Cd. Dashed curves as in Fig. 4, solid curves (RSCA-*BR*) include also recoil (*R*).

V. DISCUSSION

In Figs. 4–6 the experimental data are compared to relativistic semiclassical (RSCA) calculations carried out according to the work of Pauli, Rösel, and Trautmann.[33–35] In all three figures, the solid curves represent the net result to be compared to experiments. The dashed curves in Figs. 4 and 5 show the monopole ($l = 0$) contribution separately in order to bring out the varying contribution of the dipole ($l = 1$) and quadrupole ($l = 2$) electron continuum states. The difference between solid and dashed curves is almost completely due to the dipole term alone, which justifies the limitation to a maximum $l = 2$ in the calculations. The index B in Figs. 4–6

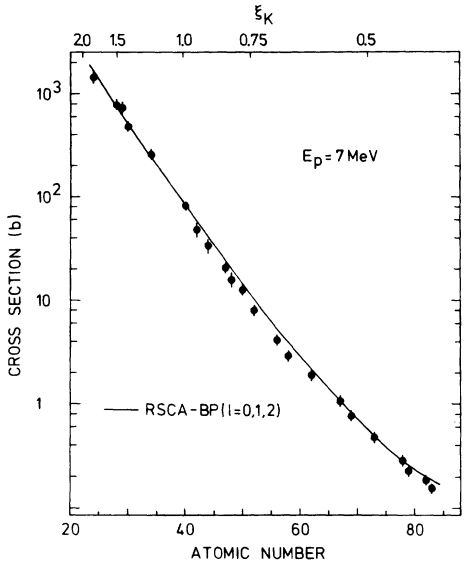

FIG. 6. Total K-shell ionization cross sections by 7-MeV protons for the range of targets from $_{24}$Cr to $_{83}$Bi. Velocity scale ξ_K and solid curve as in Fig. 4. In the calculation of these cross sections, polarization (P) as well as binding (B) by the projectile charge are taken into account.

denotes that a binding correction has been applied to the calculation, while the R in Fig. 5 denotes inclusion[35] of recoil, and the index P in Fig. 6 the correction for polarization. These corrections will be discussed below.

The data span the transition region from adiabatic ($\xi_K = 0.42$) to nonadiabatic ($\xi_K = 1.8$) collisions, and from strongly relativistic ($\alpha Z = 0.61$ for Bi) to nonrelativistic ($\alpha Z = 0.18$ for Cr) K-shell electron motion. They test, therefore, various aspects of the semiclassical description whose relative importance is changing over the data range. Dirac wave functions with $Z_{\text{eff}} = Z - 0.3$ are used for the electron in all calculations shown in Figs. 4–6. This choice will also be discussed below. The projectile is assumed, in the RSCA calculation, to move on a Rutherford hyperbola with the classically determined velocity. Thus, no additional Coulomb deflection corrections occur.

In the total K-shell cross sections σ_K (Fig. 6) one finds the by now almost standard agreement of calculation with experiment, which depends in the present situation only marginally on the applied binding and polarization corrections. As the reduced-velocity parameter ξ_K reaches values greater than 1, the data cover situations where the radial region r, which contributes most[2] to σ_K, lies outside r_K. The agreement in this region shows that the electron wave functions can be sufficiently approximated by relativistic hydrogenic wave functions, i.e., that outer screening has little effect on the shape of the radial electron wave function[11] even some distance beyond r_K.

However, the ionization probabilities in close collisions (Fig. 4) reveal certain problems. Although the RSCA calculations follow a trend still quite similar to that of the data points over more than two orders of magnitude, significant discrepancies exist between data and calculations. One first observes the size of the dipole ($l = 1$) contribution to increase from 17% of the net theoretical ionization probability at Bi to 40% at Cr. Such an increase of the dipole contribution is expected[36] as the collisions become gradually less adiabatic. At the same time, at about $\xi_K = 1$, experimental data move from below theory to above theory, exhibiting a drastically different Z dependence. At Cr, experiment is 1.7 times above calculation. We note that discrepancies are largest when the dipole contribution is largest. The significant deviations from RSCA are not limited to the scattering angles which correspond to the data of Fig. 4. Rather, they persist at backward angles for the 7-MeV points, as is shown by Fig. 5. As in the region $Z = 40$–50 in Fig. 4, the experimental points happen to almost coincide with the monopole ($l = 0$) curve with which they also share the near-isotropy with proton scattering angle. It thus appears that the deviations of the data from semiclassical theory single out the very close collisions, with impact parameters only a few times the nuclear radius, and that deviations at forward angles become most pronounced with increasing relative collision energy.

It has been shown by Trautmann and Rösel[35] that the influence on K-shell ionization probability of nuclear distortions in the projectile motion remains negligible for all scattering conditions where the elastic scattering cross section deviates by less than 50% from Rutherford scattering. We have calculated optical-model elastic cross sections using the potential parameters of Becchetti and Greenlees[26] and find, at 7 MeV and 21°, deviations of less than 6% from Rutherford cross sections between Cr and Zr. Above Zr, the deviation remains below 50% even at 90° scattering angle. We may therefore safely conclude that, although a semiclassical description of projectile motion is no longer ideally valid for our low-Z targets, the nuclear distortion effects on K-shell ionization probability remain negligible for 7-MeV scattering into the forward hemisphere. This statement can be extended to the 130° scattering at 7 MeV on Mo, Cd, and Sn. For example, the 7-MeV experimental elastic cross

section[37] on ^{106}Cd at 125° is only 10% below Rutherford. Thus, with the possible exception of the 130° points at 10 and 12 MeV, the nuclear distortions of the projectile motion cannot account for the marked deviations of the measured K-shell ionization probability from the RSCA calculated values.

We observe the largest discrepancies between experimental ionization probability and RSCA at low atomic number. However, the total K-shell cross sections in this same target range agree satisfactorily with RSCA. The problem thus resides in the close collisions where nuclear recoil[36, 38] may become important. There are as yet few numerical calculations available that include recoil.[35, 36, 38] An estimate of the recoil contribution in our experimental collision systems will therefore be preliminary. Amundsen[36] has carried out relativistic calculations of K-shell ionization probability that include recoil. In the case of 2-MeV protons on Au ($\xi_K \simeq 0.2$) he finds a reduction of at most 30% in K-shell probability due to recoil. He notes that the recoil contributions change sign at about $\xi_K = 1$, leading to an increase of K-shell ionization probability for $\xi_K > 1$ at small impact parameters. He illustrates this point by a calculation for 7-MeV protons on Mo ($\xi_K = 0.96$). The Mo data[19] he used for comparison (without actually giving the scale) are superseded by the more accurate experimental values of this work. Recoil effects have also been studied for nonrelativistic K-shell electrons (Cu, $\alpha Z = 0.21$) and slow collisions ($\xi_K < 1$) by Kleber and Unterseer.[38] These authors confirm qualitatively, by their variational approach, the semiclassical findings of Amundsen[36] and give numerical results of K-shell probability for 0.5–2.0-MeV protons on Cu. The reduction due to recoil is considerable (41% at 0.5 MeV, 21% at 2 MeV) in 180° scattering, but negligible for scattering angles below 30°. There is as yet no published calculation, including recoil, for collision systems with $\xi_K > 1$, though Trautmann and Rösel[35] have recently derived a radial form factor for their semiclassical ionization calculation that permits the inclusion of recoil effects. Our data points (Fig. 4) start to rise more steeply than the RSCA calculation precisely around $\xi_K = 1$, as one would expect for the recoil contribution. The quoted examples of numerical calculations, however, indicate that we cannot expect recoil to account for more than a 5–10% increase in K-shell ionization probability in forward scattering ($\theta_p \leq 35°$), while at Cr ($\xi_K = 1.8$) experiment is 1.7 times above the RSCA value. The data of Fig. 5 and a numerical calculation with the radial form factor of Trautmann and Rösel including recoil[35] corroborate the foregoing conclusions. The ionization probability P_K changes by less than 1% in all cases given in Figs. 4 and 5, except for 130° scattering. Here, the largest reduction of P_K by recoil occurs for scattering at 7 MeV on Sn ($\xi_K = 0.78$), where it amounts to 12%. Smaller reductions of P_K in 130° scattering are found for $\xi_K = 0.96$ (10%, Mo at 7 MeV) and $\xi_K = 1.03$ (8%, Sn at 12 MeV). Thus in the approximation of Ref. 35, represented by the solid curves in Fig. 5, the effect of recoil tends to zero at a value ξ_K somewhat above unity. The data of Fig. 5 show no clear indication of this trend but, at 7 MeV, are still quite uniformly below RSCA. The remaining difference between data and semiclassical calculation, though slightly reduced, may therefore not be attributed to recoil.

Possible perturbations of the isotropic K x-ray emission by K-L-shell double ionization can readily be excluded as a reason for the rise in ionization probability at low Z. The estimate, with the formula given by Madison and Merzbacher,[39] yields $P_{KL}/P_K \simeq 1.5\times10^{-2}$, with P_{KL} the K-L double ionization probability for 7-MeV protons with zero impact parameter on Cr. We therefore believe the assumption of isotropic x-ray emission as well as unperturbed K-shell fluorescence yield ω_K to be well justified.

Ionization by charge transfer is also not expected to account for the rise in ionization probability above RSCA for the $\xi_K > 1$ collisions. For 7-MeV protons on Ar, K-shell ionization by charge transfer to the proton has a cross section of $\sigma_{CK} \simeq 10$ b, and is decreasing for higher proton energies.[40, 41] This is approximately 0.2% of the total K-shell ionization cross section. As the p+Cr collision system is still more asymmetric, the importance of charge transfer in K-vacancy production is even more reduced. The agreement of the total K-shell ionization cross section with the RSCA Coulomb ionization calculation down to Cr supports this conclusion. The impact-parameter dependence of charge-transfer probability being flat, one would expect it, if large, to be visible at both small and large impact parameters and thus in total cross sections.

The choice of the electron wave functions thus remains as the most critical point of the semiclassical calculation. Aashamar and Kocbach[11] have compared K-shell cross sections and ionization probabilities calculated with either nonrelativistic hydrogenic (H) or Hartree-Fock-Slater (HFS) free-electron wave functions. They find that the realistic HFS potential of Cu approaches the energy-shifted Coulomb potential for radii in the K-shell spatial region, as could be expected from the discussion of outer screen-

ing by Merzbacher and Lewis.[10] As a consequence, Aashamar and Kocbach find both free and bound hydrogenic and HFS radial electron wave functions to be virtually indistinguishable at radii in the K-shell region. Appreciable deviations in the free wave functions start only at radii several times the K-shell radius, r_K, the zero energy and $l>0$ orbital angular momentum states of the free electron being the most sensitive ones. The choice of hydrogenic electron wave functions thus appears justified in adiabatic collisions ($\xi_K<1$), where ionization takes place in the interior of the K shell. This conclusion holds analogously also for relativistic K-shell electrons. Pauli *et al.*[12] have demonstrated this point in a semiclassical K-shell calculation for 2-MeV protons on Ag ($\xi_K=0.45$) employing relativistic Hartree-Fock wave functions for both the bound and free-electron states. The K-shell ionization probability is reproduced within experimental error by the calculation with Hartree-Fock wave functions, and within 10% when relativistic hydrogenic wave functions are employed. This difference can probably be attributed to the imperfect reproduction of the free-electron Hartree-Fock wave function by the hydrogenic solution at the lowest electron energies.[11,12,35] The data for $\xi_K<1$ ($Z>40$) in Fig. 4 show a quite similar behavior: The RSCA calculation with relativistic hydrogenic electron wave functions moderately overestimates (from 20 to 35%) the data. It is thus likely that here too the hydrogenic approximation is responsible for this small discrepancy. The hydrogenic approximation is expected[13] to deteriorate for collisions with $\xi_K>1$ where ionization takes place in more distant radial regions. In fact, the data of Fig. 4 show a pronounced rise above hydrogenic RSCA theory just for $\xi_K>1$ ($Z<40$). Moreover, a first attempt at an RSCA calculation with Hartree-Fock electron wave functions by Trautmann and Rösel[35] has shown that the K-shell ionization probability in just this data range is quite sensitive to the choice of the electron wave functions, in line with the findings of Aashamar and Amundsen[13] who generally obtained results even more sensitive for fast collisions in very light collision systems ($Z=6$ and 10) with the exception, however, of the range $1.4\leq\xi_K\leq1.8$. It is likely that the use of appropriate nonhydrogenic wave functions will lift the discrepancy in our low-Z K-shell ionization probabilities at 7 MeV. There are as yet no numerical values available[42] that would cover our whole data interval $24\leq Z\leq83$. It also remains to be seen to what degree the use of the Hartree-Fock wave functions modifies the relativistic hydrogenic results for $\xi_K<1$ in Fig. 4.

A discussion of binding effects in the electron wave function may be in place although such effects are small in our whole data range. Their presence is, however, brought out quite clearly in Fig. 7, where the experimental K-shell cross sections σ_K and ionization probabilities P_K of Figs. 4 and 6 are given, divided by the corresponding RSCA values as calculated with relativisitic hydrogenic wave functions, and with no binding corrections incorporated. A characteristic pattern emerges: Starting from small values of ξ_K (high atomic number), the ratios in both σ_K and P_K increasingly fall below unity, reach a minimum of about 0.7 at $\xi_K\simeq0.7$–0.8, and then rise for $\xi_K>1$. The behavior of the σ_K ratios differs from that of the P_K ratios for $\xi_K>1$ in that the former rise towards unity while the latter reach almost 1.6. The qualitative trend of the points in Fig. 7(a) can be understood[28,29] as the combined effect of binding and polarization of the K electron by the projectile charge: at $\xi_K<0.6$ binding dominates so that the K-shell cross section falls below RSCA, the more so the larger the charge ratio Z_1/Z_2, i.e., the larger ξ_K. At still higher ξ_K values, the region of the dominant contribution to σ_K moves outward and the projectile increasingly polarizes the K-shell electron distribution, which eventually overrides binding. In still more distant collisions, taking the just described binding (B) and polarization (P) distortions into account in the perturbed stationary-state approximation employed by Basbas *et al.*[29] one obtains the solid curves in Figs. 6 and 7(a). We find that no quantitative agreement with the size of the distorting effects on the electron binding energy is obtained, but that the trends contained in the σ_K data are well reproduced. A correction procedure for probabilities P_K analogous to Ref. 29 is not available. A simple estimate may, however, be made for the adiabatic region $\xi_K<1$. It is readily shown that, upon equating the internuclear distance with the impact parameter, the effective perturbed K-shell binding energy $E_K^{\rm eff}$ of Basbas *et al.*[28,29] approaches, for adiabatic collisions with near-zero impact parameter, the unperturbed united-atom binding energy $E_K(Z+1)$. Amundsen[36] has generalized this conclusion to arbitrary electron wave functions. We have therefore used $E_K^{\rm eff}=E_K(Z+1)$ for both the momentum transfer and the Dirac wave function in the calculation of the ionization probability P_K. This yields the solid curves RSCA-B in Figs. 4 and 7(b), and RSCA-BR in Fig. 5. For lack of a more appropriate procedure, and as the reduction in P_K remains below 10% throughout, we have employed the above estimate also in the transition region $1\leq\xi_K\leq2$ when establishing the RSCA-B

curve of Fig. 4. One ought to keep in mind, however, that the binding correction based on Refs. 28 and 29 has previously been shown[32,43] to be insufficient above $\xi_K \simeq 0.55$; and that the expected polarization effects are not taken into account in our estimate for P_K. As in the case of the K-shell cross sections σ_K the binding correction underestimates the actual difference between data and RSCA, for $\xi_K \leq 1$, as is seen from Fig. 7(b). While our previous discussion of wave-function effects leads us to attribute the remaining difference to the use of Dirac wave functions, Goldberg and Ponce[44] have traced such a trend back to the use of a time-independent target nuclear charge in Refs. 6, 28, and 29. They propose to employ an optimized time-dependent charge, very much like in the work of Jakubassa[45] for relativistic collision systems. Both these methods are closely related to the as yet nonrelativistic variational approach by Kleber and Unterseer.[38] It remains to be seen whether quantitative agreement with the actual electron distortion effects can be obtained by the calculations of Refs. 38, 44, and 45.

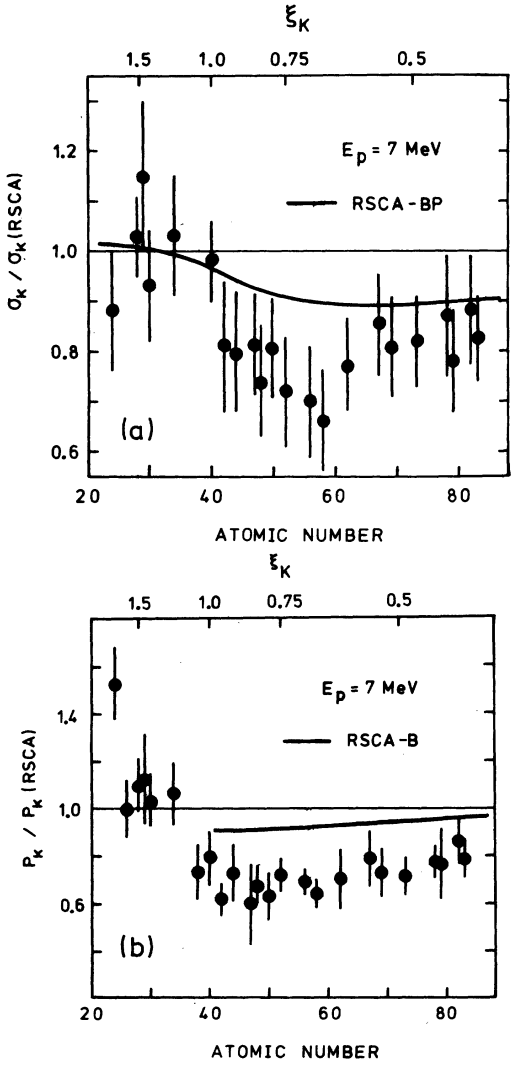

FIG. 7. Effect of finite-projectile-charge corrections on (a) K-shell ionization cross sections (σ_K) of Fig. 6, and (b) ionization probabilities (P_K) of Fig. 4. The data points give the ratio of experimental and corresponding uncorrected RSCA values (see text). The solid curves show theoretical ratios, with finite-charge-corrected values RSCA-BP (a), and RSCA-B (b) instead of the experimental ones, and where B labels the binding and P the polarization correction.

VI. CONCLUSION

The preceding discussion of ionization data in central collisions has shown some significant deviations from the current semiclassical description with relativistic hydrogenic wave functions, especially for the nonadiabatic situations at low atomic number. It has been shown that nuclear recoil does not account for more than a very small fraction of the deviations. The distortion of the electron wave function by the projectile charge, though small, is clearly present in both the K-shell total cross sections and the central collision ionization probabilities. Its description based on the perturbed-stationary-state approximation underestimates the real effect somewhat. The most pronounced deficiency in the description of the data consists, however, in the use of hydrogenic electron wave functions, particularly in the nonadiabatic low-Z region. The data change from below the relativistic hydrogenic semiclassical calculation to above this calculation upon transition to the nonadiabatic collisions, in accordance with the recent prediction that wave-function effects have precisely this sign and will be largest in fast collisions with light atoms. It will therefore be interesting to follow the present data series to targets of still lower atomic number.

ACKNOWLEDGMENTS

We are particularly indebted to M. Pauli, F. Rösel, D. Trautmann, and G. Baur who have kindly provided us with their RSCA computer code already at an early stage. Moreover, we have profited from discussions on inner-shell ionization we had on various occasions and from frequent help with the computing. We also thank P. A. Amundsen for informing us of his work on wave-function effects before its publication, and J. F. Reading and W. Brandt for discussions on charge transfer and projectile charge effects. H. Paetz gen. Schieck has helped generously with the beam from

the Köln polarized ion source. We finally thank E. Friederichs who carried out some of the numerical calculations of double scattering effects. This work was supported by Deutsche Forschungsgemeinschaft and by Bundesministerium für Forschung und Technologie, Bonn, Germany.

APPENDIX

We give here the data displayed in Figs. 4–6 (see Table IV).

TABLE IV. The data displayed in Figs. 4–6.

Target	E_p (MeV)	θ_p (deg)	b (fm)[a]	$P_K(\theta_p)$[b]	$\sigma_K(E_p)$ (b)[b]
Cr	7	13	22 ± 14	7.3 ± 0.7(−3)	1.41 ± 0.20(3)
Fe		13	23 ± 14	4.1 ± 0.5(−3)	
Ni		21	15 ± 7	3.8 ± 0.4(−3)	7.78 ± 0.62(2)[c]
Cu		21	16 ± 7	3.6 ± 0.6(−3)	7.32 ± 0.95(2)
Zn		21	17 ± 7	3.1 ± 0.3(−3)	4.30 ± 0.52(2)
Se		21	19 ± 7	2.2 ± 0.3(−3)	2.56 ± 0.31(2)
Sr		21	21 ± 12	1.1 ± 0.2(−3)	
Zr		21	22 ± 9	9.7 ± 1.1(−4)	8.70 ± 0.84(1)
Mo		15	33 ± 17	6.4 ± 0.7(−4)	4.79 ± 0.77(1)
		130	2^{+3}_{-2}	5.1 ± 1.7(−4)	
Ru		30	17 ± 8	6.2 ± 1.1(−4)	3.33 ± 0.53(1)
Ag		30	18 ± 8	3.9 ± 1.2(−4)	2.05 ± 0.33(1)
Cd	7	30	18 ± 9	4.1 ± 0.5(−4)	1.57 ± 0.25(1)
	7.138	130	2^{+3}_{-2}	4.0 ± 1.4(−4)	
Sn	7	15	39 ± 19	3.2 ± 0.5(−4)	1.24 ± 0.20(1)
	7.138	130	2^{+3}_{-2}	3.4 ± 0.5(−4)	
	10	15	28 ± 14	4.7 ± 0.5(−4)	
		130	2 ± 2	5.1 ± 3.7(−4)	
	12	15	23 ± 12	5.4 ± 0.5(−4)	
		130	1^{+2}_{-1}	6.4 ± 1.1(−4)	
Te	7	30	20 ± 9	3.1 ± 0.3(−4)	8.02 ± 1.3(0)
Ba		30	21 ± 10	2.2 ± 0.2(−4)	4.17 ± 0.67(0)
Ce		30	22 ± 10	1.7 ± 0.2(−4)	2.90 ± 0.46(0)
Sm		35	20 ± 9	1.4 ± 0.3(−4)	1.89 ± 0.23(0)
Ho		35	22 ± 9	1.1 ± 0.2(−4)	1.06 ± 0.13(0)
Tm		35	23 ± 9	9.3 ± 1.2(−5)	7.71 ± 0.93(−1)
Ta		35	24 ± 10	7.2 ± 0.8(−5)	4.76 ± 0.57(−1)
Pt		35	25 ± 10	6.1 ± 0.5(−5)	2.83 ± 0.34(−1)
Au		35	26 ± 10	5.7 ± 1.2(−5)	2.21 ± 0.27(−1)
Pb		35	27 ± 10	5.7 ± 0.6(−5)	1.84 ± 0.24(−1)
Bi		35	27 ± 10	5.0 ± 0.5(−5)	1.55 ± 0.17(−1)

[a] Uncertainty combined from Δb_1 and Δb_2 (see text, Sec. IV).
[b] Numbers in brackets give powers of 10.
[c] We give here the value from Ref. 31 because it is more accurate.

[1] R. K. Gardner and T. J. Gray, At. Data Nucl. Data Tables 21, 515 (1978).
[2] J. Bang and J. M. Hansteen, Kgl. Danske Vidensk. Selsk. Mat. Fys. Medd. 31, no. 13 (1959).
[3] W. Brandt, K. W. Jones, and H. W. Kraner, Phys. Rev. Lett. 30, 351 (1973).
[4] E. Laegsgaard, J. U. Andersen, and L. C. Feldman, Phys. Rev. Lett. 29, 1206 (1972).

[5]D. L. Clark, T. K. Li, J. M. Moss, G. W. Greenlees, M. E. Cage, and J. H. Broadhurst, J. Phys. B 8, L378 (1975).
[6]J. U. Andersen, E. Laegsgaard, M. Lund, and C. D. Moak, Nucl. Instrum. Methods 132, 507 (1976).
[7]J. U. Andersen, L. Kocbach, E. Laegsgaard, M. Lund, and C. D. Moak, J. Phys. B 9, 3247 (1976).
[8]E. Laegsgaard, J. U. Andersen, and M. Lund, in *Proceedings of the 10th International Conference on Physics of Electronic and Atomic Collisions, Paris, 1977*, edited by G. Watel (North-Holland, Amsterdam, 1978), p. 353.
[9]E. Laegsgaard, J. U. Andersen, and F. Høgedal, Nucl. Instrum. Methods 169, 293 (1980).
[10]E. Merzbacher and H. W. Lewis, in *Handbuch der Physik*, edited by S. Flügge (Springer, Berlin, 1958), Vol. 34, p. 166.
[11]O. Aashamar and L. Kocbach, J. Phys. B 10, 869 (1977).
[12]M. Pauli, F. Rösel, and D. Trautmann, Phys. Lett. 67A, 28 (1978).
[13]K. Aashamar and P. A. Amundsen, J. Phys. B 14, 483 (1981).
[14]K. H. Weber and F. Bell, Phys. Rev. A 16, 1075 (1977).
[15]W. Jank, F. Bell, and K. H. Weber, Phys. Lett. 66A, 293 (1978).
[16]S. Röhl, S. Hoppenau, and M. Dost, Phys. Rev. Lett. 43, 1300 (1979); and (unpublished).
[17]J. F. Chemin, S. Andriamonje, J. Roturier, B. Saboya, R. Gayet, and A. Salin, Phys. Lett. 67A, 116 (1978).
[18]J. F. Chemin, S. Andriamonje, S. Denagbe, J. Roturier, B. Saboya, and J. P. Thibaud, Phys. Rev. A 15, 1851 (1977).
[19]S. Röhl, S. Hoppenau, and M. Dost, in *Proceedings of the 10th International Conference on Physics of Electronic and Atomic Collisions, Paris, 1977*, edited by G. Watel (North-Holland, Amsterdam, 1978), p. 76.
[20]M. Dost, S. Hoppenau, J. Kising, and S. Röhl, in *Proceedings of the 11th International Conference on Physics of Electronic and Atomic Collisions*, edited by K. Takayanagi and N. Oda (North-Holland, Amsterdam, 1979), contributed papers, p. 680.
[21]M. Dost, Nucl. Instrum. Methods 169, 305 (1980).
[22]W. Bambynek, B. Crasemann, R. W. Fink, H. U. Freund, H. Merk, C. D. Swift, R. E. Price, and P. Venugopala Rao, Rev. Mod. Phys. 44, 716 (1972).
[23]E. Friederichs, Diplomarbeit, University of Köln (unpublished).
[24]K. Alder, A. Bohr, T. Huus, B. Mottelson, and A. Winther, Rev. Mod. Phys. 28, 432 (1956).
[25]F. K. McGowan and P. H. Stelson, Phys. Rev. 109, 901 (1958).
[26]F. D. Becchetti, Jr. and G. W. Greenlees, Phys. Rev. 182, 1190 (1969).
[27]N. Bohr, Kgl. Danske Vidensk. Selsk. Mat. Fys. Medd. 43, No. 8 (1948).
[28]G. Basbas, W. Brandt, and R. Laubert, Phys. Rev. A 7, 983 (1973).
[29]G. Basbas, W. Brandt, and R. Laubert, Phys. Rev. A 17, 1655 (1978).
[30]G. A. Bissinger, S. M. Shafroth, and A. W. Waltner, Phys. Rev. A 5, 2046 (1972).
[31]R. Akselsson and T. B. Johannsson, Z. Phys. 266, 245 (1974).
[32]A. Berinde, C. Deberth, I. Neamu, C. Protop, N. Scintei, V. Zoran, M. Dost, and S. Röhl, J. Phys. B 11, 2875 (1978).
[33]M. Pauli and D. Trautmann, J. Phys. B 11, 667 (1978).
[34]M. Pauli, F. Rösel, and D. Trautmann, J. Phys. B 11, 2511 (1978).
[35]D. Trautmann and F. Rösel, Nucl. Instrum. Methods 169, 259 (1980).
[36]P. A. Amundsen, J. Phys. B 11, 3197 (1978).
[37]E. Abramson, R. A. Eisenstein, I. Plesser, and Z. Vager, Nucl. Phys. A138, 609 (1969).
[38]M. Kleber and K. Unterseer, Z. Phys. A 292, 311 (1979).
[39]Don H. Madison and E. Merzbacher, in *Atomic Inner-Shell Processes*, edited by B. Crasemann (Academic, New York, 1975), Vol. 1, p. 1, Eq. (76).
[40]J. R. Macdonald, C. L. Cocke, and W. W. Eidson, Phys. Rev. Lett. 32, 648 (1974).
[41]A. L. Ford, J. F. Reading, and R. L. Becker, J. Phys. B 12, 2905 (1979).
[42]D. Trautmann, F. Rösel, and G. Baur (private communication).
[43]V. Zoran, J. Phys. B 12, 2179 (1979).
[44]E. C. Goldberg and V. H. Ponce, Phys. Rev. A 22, 399 (1980).
[45]D. H. Jakubassa, Z. Phys. 293, 281 (1979).